P-T Phase Diagram and Gold Valence State of the Perovskite-Type Mixed-Valence Compounds $Cs_2Au_2X_6$ (X = Cl, Br, and I) under High Pressures

N. Kojima,*,†,‡ M. Hasegawa,† H. Kitagawa,§ T. Kikegawa,|| and O. Shimomura||

Contribution from the Department of Chemistry, Faculty of Science, Kyoto University, Kyoto 606, Japan, Institute for Molecular Science, Okazaki 444, Japan, and National Laboratory for High Energy Physics, Tsukuba 305, Japan

Received August 13, 1993. Revised Manuscript Received April 20, 1994®

Abstract: We have elucidated the structural P-T phase diagram of $Cs_2Au_2X_6$ (X = Cl, Br, and I) under high pressures and high temperatures for the first time. When the pressure is applied at room temperature, the $Cs_2Au_2X_6$ (X = Cl, Br, and I) compounds undergo a tetragonal-to-tetragonal phase transition at 11, 9, and 5.5 GPa, respectively. This transition is regarded as a band Jahn-Teller transition driven by the $Au^{I,III} \rightarrow Au^{II}$ transition. The cubic perovskite structure appears under high pressures and high temperatures for all three compounds. For $Cs_2Au_2Br_6$ and $Cs_2Au_2I_6$, the cubic phase could be obtained as a metastable state at room temperature and ambient pressure. The Au valence states in the second tetragonal phase and the cubic phase are considered to be Au^{II}.

Since the discovery of high-T_c superconductors such as $La_{2-x}Ba_xCuO_4$[1] and $Ba_{1-x}K_xBiO_3$,[2] mixed valence systems having perovskite-type structure have become of great interest. In these systems, interesting physical properties such as superconductivity remarkably depend on the valence state and the crystal structure.

From the viewpoint of the bipolaron model, the insulating $BaBiO_3$, which is the parent compound of the superconductors Ba_{1-x}(K or Rb)$_xBiO_3$ and $BaBi_{1-x}Pb_xO_3$, is regarded as an on-site bipolaron system (i.e. negative U system) where the bipolarons form a three-dimensional lattice and localize at the Bi^{III} site. According to recent theory,[3,4] an unusual superconductor due to the Bose condensation of bipolarons is expected under some electron-phonon coupling constant λ, while in the large limit of λ, a bipolaronic insulator occurs.

$Cs_2Au_2X_6$ (X = Cl, Br, and I) compounds also have a mixed valence system having a perovskite-type structure. According to the XPS and the ^{197}Au Mössbauer measurements,[5,6] these compounds exhibit the $Au^{I,III}$ mixed valency. The crystals have a tetragonal perovskite structure with the space group *I4/mmm*,[7-9] which is shown in Figure 1. Its structure consists of a three-dimensional metal-halogen framework formed by elongated octahedra with Au^{III} and compressed octahedra with Au^{I} sharing their corners. Consequently, the breathing-mode-type distortion of AuX_6 octahedra is present in this system. These characteristic properties of crystal structure and mixed valency are quite similar to those of $BaBiO_3$.

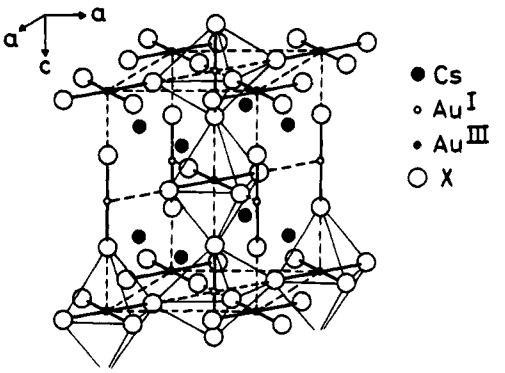

Figure 1. Crystal structure of $Cs_2Au_2X_6$ (X = Cl, Br, and I).

From this viewpoint, we have investigated the physical properties and the crystal structure of $Cs_2Au_2X_6$.[5,6,10-17]

Recently, we have found that $Cs_2Au_2I_6$ under high pressures undergoes a semiconductor-to-metal transition (P = 4.5 GPa, T = room temperature (r.t.)) and a metal-to-metal transition (P = 6.5 GPa, T $\approx$ 330 K) and the second metallic phase appearing at high pressure and high temperature can be obtained at r.t. and ambient pressure (a.p.) as a metastable state.[10,11] In the

† Kyoto University.

‡ Current address: Department of Pure and Applied Sciences, College of Arts and Sciences, University of Tokyo, Komaba, Meguro-ku, Tokyo 153, Japan.

§ Institute for Molecular Science.

|| National Laboratory for High Energy Physics.

® Abstract published in *Advance ACS Abstracts*, November 1, 1994.

(1) Bednorz, J. G.; Müller, K. A. *Z. Phys. B.* **1986**, *64*, 189-193.

(2) Cava, R. J.; Batlogg, B.; Krajewski, J. J.; Farrow, R.; Rupp, L. W., Jr.; White, A. E.; Short, K.; Peck, W. F.; Kometani, K. *Nature* **1988**, *332*, 814-816.

(3) Chakraverty, B. K. *J. Phys. Lett.* **1979**, *40*, L99-100.

(4) Alexandrov, A.; Ranninger, J. *Phys. Rev. B* **1981**, *23*, 1796-1801.

(5) Kitagawa, H.; Kojima, N.; Nakajima, T. *J. Chem. Soc., Dalton Trans.* **1991**, 3121-3125.

(6) Kitagawa, H.; Kojima, N.; Sakai, H. *J. Chem. Soc., Dalton Trans.* **1991**, 3211-3215.

(7) Elliott, N.; Pauling, L. *J. Am. Chem. Soc.* **1938**, *60*, 1846-1851.

(8) Brauer, B.; Sleater, G. *J. Less-Common Metals* **1970**, *21*, 283-291.

(9) Tindemans v. Eijndhoven, J. C. M.; Verschoor, G. C. *Mater. Res. Bull.* **1974**, *9*, 1667-1670.

(10) Kojima, N.; Kitagawa, H.; Ban, T.; Amita, F.; Nakahara, M. *Solid State Commun.* **1990**, *73*, 743-745.

(11) Kojima, N.; Kitagawa, H.; Ban, T.; Amita, F.; Nakahara, M. *Synth. Met.* **1991**, *41-43*, 2347-2350.

(12) Kitagawa, H.; Sato, H.; Kojima, N.; Kikegawa, T.; Shimomura, O. *Synth. Metals* **1991**, *41-43*, 1953-1956; *Solid State Commun.* **1991**, *78*, 989-995.

(13) Kitagawa, H.; Kojima, N.; Matsushita, N.; Ban, T.; Tsujikawa, I. *J. Chem. Soc., Dalton Trans.* **1991**, 3115-3119.

(14) Kojima, N.; Kitagawa, H.; Kikegawa, T.; Shimomura, O.; Takahashi, H.; Mori, N. *Proc. Int. Conf. High Pressure Sci. Technol. (Bangalore)* **1991**, 295-297.

(15) Kojima, N.; Tanaka, A.; Sato, H.; Kitagawa, H.; Kikegawa, T.; Shimomura, O. *Jpn. J. Appl. Phys.* **1993**, *32*, 51-53.

(16) Kojima, N.; Amita, F.; Kitagawa, H.; Sakai, H.; Maeda, Yu. *Nucl. Instrum. Methods B* **1993**, *76*, 321-322.

(17) Kitagawa, H.; Kojima, N.; Takahashi, H.; Mori, N. *Synth. Met.* **1993**, *55-57*, 1726-1729.

0002-7863/94/1516-11368$04.50/0

metallic region of $Cs_2Au_2I_6$, we have found a tetragonal-to-tetragonal phase transition ($P \approx 5.5$ GPa, T = r.t.) and a tetragonal-to-cubic phase transition ($P = 6.8$ GPa, $T \approx 350$ K) by means of X-ray diffraction measurement under high pressures.[13] However, the detailed P−T phase diagram of $Cs_2Au_2I_6$ has not been elucidated.

For the case of $Cs_2Au_2Cl_6$, the single-crystal X-ray diffraction measurement under high pressures has been performed by Denner et al.[18] According to them, with increasing pressure the Cl ions shift gradually toward the midpoint of the Au ions which is attained at 5.2 GPa. Therefore, they have indicated that the Au sites become indistinguishable and the valence state of Au is Au^{II} above 5.2 GPa. However, ^{197}Au Mössbauer spectra[19,20] and Raman spectra[21] of $Cs_2Au_2Cl_6$ under high pressures have shown that the Au^{I} and Au^{III} states are clearly distinguishable even at 6.8 and 8.0 GPa, respectively. These discrepancies have not yet been made clear.

For the case of $Cs_2Au_2Br_6$, the P−T phase diagram is not known at all.

The purpose of this paper is to elucidate the P−T phase diagram for all the title compounds and to discuss the relationship between the crystal structure and the Au valence state.

Experimental Section

All the title compounds were prepared by the methods described in our previous papers.[5,13] The single crystals or polycrystals were pulverized for powder X-ray diffraction measurement.

The structure analysis of these compounds was performed by the energy-dispersive X-ray diffraction method using the high-temperature and high-pressure apparatus,[22] called MAX 80 or MAX 90, with synchrotron radiation (SR) in the National Laboratory for High Energy Physics (KEK). The high-pressure apparatus is a cubic anvil type whose anvils compress a boron−epoxy cube containing a sample capsule. The anvils used were made of tungsten carbides having an edge length of 6 mm or sintered diamonds having an edge length of 3 mm or 4 mm, which generate pressures up to 7, 14, or 11 GPa, respectively. Ethanol or kerosene was used as a fluid pressure-transmitting medium in the Teflon capsule. The pressure was determined by measuring the lattice constants of NaCl set in the boron−epoxy cube. The sample was heated by a disk-like graphite heater and its temperature was measured by an alumel−chromel thermocouple. The sample assembly used is shown in Figure 2. The diffracted X-ray was detected by a solid-state detector (pure Ge) mounted on the arm of the goniometer. The mean measuring time was about 15 min. The position and intensity of each diffraction peak were obtained by least-squares Gaussian fitting to its profile. The lattice parameters were determined by a least-squares fit to the measured positions where $2\theta = 2.5-4.5°$.

Results

$Cs_2Au_2I_6$. X-ray diffraction patterns of $Cs_2Au_2I_6$ were measured in the region of a.p. to 10.4 GPa and r.t. to 240 °C.

Figure 3 shows the pressure depedence of the X-ray diffraction profile of $Cs_2Au_2I_6$ at r.t. Among these diffraction peaks, (211) and (103) are the reflections caused by the distortion of the I ions from the midpoint between the Au^{I} and Au^{III} ions. As seen in Figure 3, the intensities of the (211) and (103) reflections decrease with increasing pressure, which implies that the bridging I ions approach the midpoint of the Au^{I} and Au^{III} ions with increasing pressure.

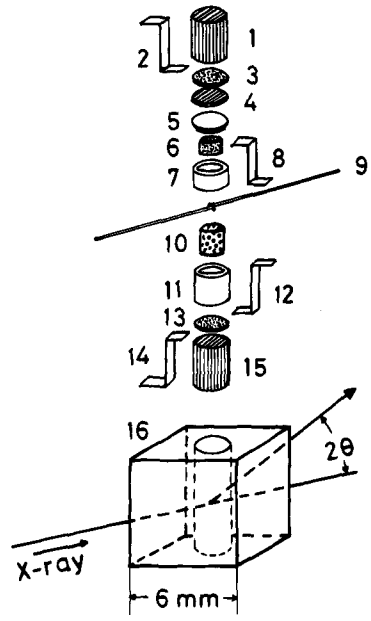

Figure 2. Sample assembly used for the X-ray diffraction measurements under high pressures: (1, 15) pyrophyllite plug; (2, 8, 12, 14) Au lead foil; (3, 13) graphite disk; (4) pyrophyllite disk; (5) Teflon cap; (6) sample with pressure medium; (7, 11) Teflon capsule; (9) thermocouple; (10) NaCl; and (16) boron−epoxy cube.

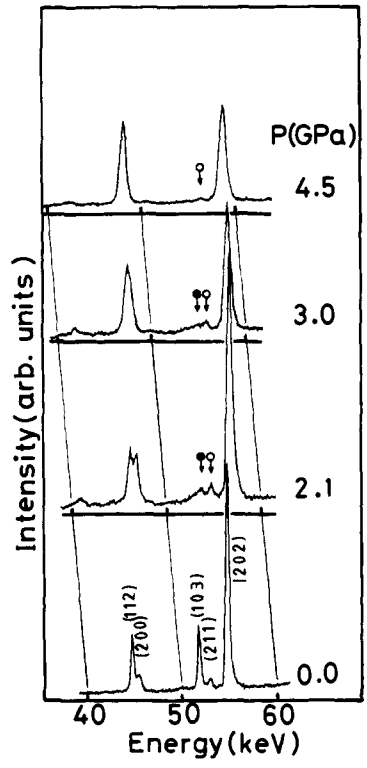

Figure 3. Pressure dependence of the (211) and (103) reflections of $Cs_2Au_2I_6$ at r.t. Here, $2\theta = 3.80°$. Open and closed circles with arrows denote the (211) and (103) reflections, respectively.

Figure 4 shows the pressure dependence of the lattice constants, a and c, at r.t. With increasing pressure up to 5.2 GPa, the lattice constants, a and c, decrease monotonously showing concave curvatures. Above 5.7 GPa, the gradient of contraction of the c-axis becomes rather smaller, while that of the a-axis becomes larger. In the pressure region between 5.6 and 6.4 GPa, a tetragonal-to-tetragonal phase transition occurs

(18) Denner, W.; Schulz, H.; D'Amour, H. *Acta Crystallogr. A* **1979**, *35*, 360−365.
(19) Stanek, J.; Hafner, S. S.; Schulz, H. *Phys. Lett. A* **1980**, *76*, 333−334.
(20) Stanek, J. *J. Chem. Phys.* **1982**, *76*, 2315−2320.
(21) Tanino, H.; Syassen, K.; Wang, Z.; Hanfland, M.; Takahashi, K. *Proc. Int. Conf. High Pressure Sci. Technol. (Parderborn)* **1989**, 183−185.
(22) Shimomura, O. *Phys. B* **1986**, *139 & 140*, 292−300.

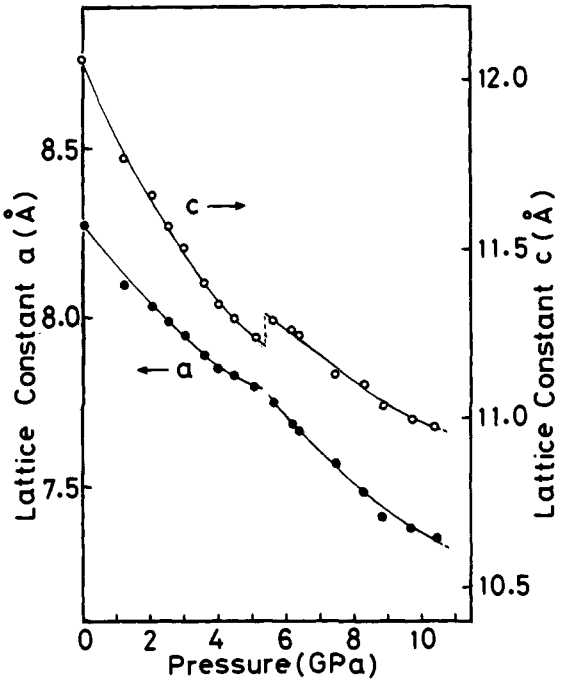

Figure 4. Pressure dependence of the lattice constants of $Cs_2Au_2I_6$ at r.t.

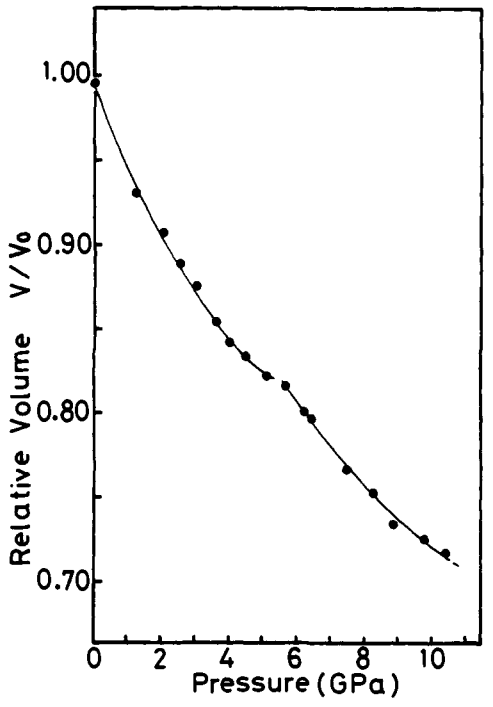

Figure 5. Pressure dependence of the volume of $Cs_2Au_2I_6$ at r.t. The volume is normalized by that (V_0 = 829.81 Å^3) at a.p.

where the *c*-axis elongates discontinuously and the reflections belonging to the lower and the higher pressure phases clearly coexist. The distinct coexistence of two phases in the vicinity of the phase transition is due to the nature of the first-order transition, as well as the pressure distribution in the sample, which is expected to be small for the fluid pressure-transmitting medium. For the case of the relative volume shown in Figure 5, the gradient of the volume contraction changes obviously at the transition pressure.

Figure 6 shows the pressure dependence of the axial ratio $2^{1/2}a/c$, which indicates the distortion of the tetragonal lattice. The cubic lattice is realized at $2^{1/2}a/c = 1$. With increasing

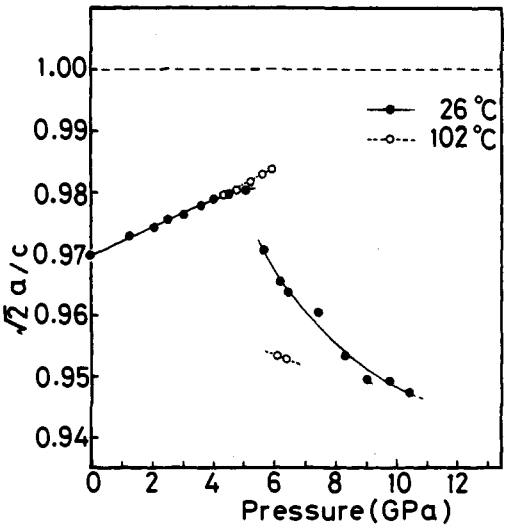

Figure 6. Pressure dependence of the axial ratio $2^{1/2}a/c$ of $Cs_2Au_2I_6$.

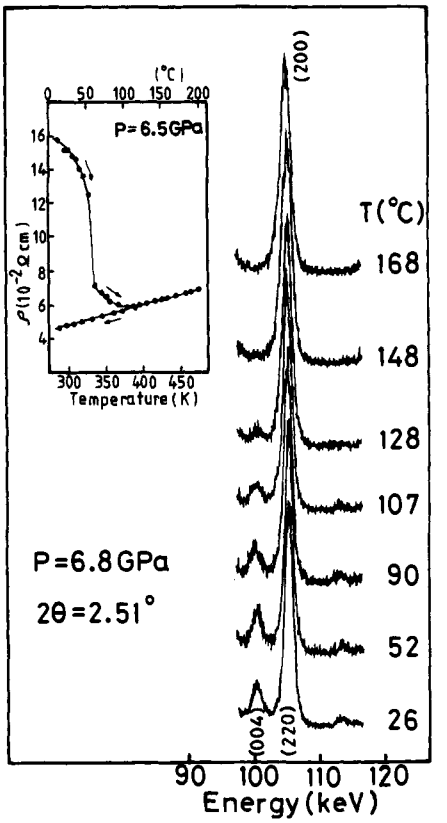

Figure 7. Temperature dependence of the (004) and (220) reflections of $Cs_2Au_2I_6$ at 6.8 GPa. Here, 2θ = 2.51°. The inset shows the temperature dependence of the electrical resistivity of $Cs_2Au_2I_6$ at 6.5 GPa (ref 10). The sample was first heated to 200 °C and then cooled to r.t.

pressure up to 5.5 GPa, $2^{1/2}a/c$ increases from 0.969 to 0.980. However, it drops abruptly from 0.980 to 0.970 at the tetragonal-to-tetragonal transition. Above the transition point, $2^{1/2}a/c$ decreases from 0.970 to 0.947 with increasing pressure from 5.7 to 10.4 GPa. The drop in $2^{1/2}a/c$ due to the tetragonal-to-tetragonal transition at 102 °C is larger than that at r.t.

Figure 7 shows the temperature dependence of the (004) and (220) reflections of $Cs_2Au_2I_6$ at 6.8 GPa. As the temperature is increased at 6.8 GPa, the (004) reflection begins to diminish between 52 and 90 °C, and then disappears at about 150 °C without a change in its energy position. The (002) and (112) reflections also disappear at about 150 °C. The reflections such

as (220), due to the interplanar spacing in the a_1a_2 plane, remain unchanged in their intensities and energy positions in this process. The diffraction pattern at 6.8 GPa and 167 °C is satisfactorily explained by the cubic perovskite structure ($Pm\bar{3}m$) with a = 5.370(5) Å. These results imply that the Au−Au distance along the c-axis contracts discontinuously and becomes equal to that in the a_1a_2-plane at the tetragonal II-to-cubic transition.

Now, we investigate the relationship between the tetragonal-to-cubic transition and the behavior of the resistivity. According to our resistivity measurement for $Cs_2Au_2I_6$ under high pressures,[10] $Cs_2Au_2I_6$ undergoes a pressure-induced semiconductor-to-metal transition at P = 4.5 GPa and T = r.t. Moreover, as shown in the inset of Figure 7,[10] when the temperature is increased at 6.5 GPa, the resistivity decreases, drops steeply at about 60 °C, and then increases linearly above about 130 °C, which implies that $Cs_2Au_2I_6$ has two metallic phases and the second metallic phase appears at P = 6.5 GPa and $T \approx$ 60 °C. Comparing the behavior of the resistivity with the X-ray diffraction profiles in the vicinity of the tetragonal-to-cubic phase transition, the drastic drop in the resistivity at about 60 °C and the linear increase in the resistivity above 130 °C are attributed to the appearance of the cubic phase and the disappearance of the tetragonal II phase, respectively.

In the cooling process, the resistivity decreases linearly as the temperature is cooled down to r.t., which implies that the second metallic phase (phase III) can be stable at P = 6.5 GPa and T = r.t. Moreover, this metallic phase could be obtained as a metastable phase at r.t. and a.p. by decreasing the pressure.[10] This metastable phase was rather unstable and its resistivity at r.t. and a.p. increased gradually from 5×10^{-2} to 1×10^{7} Ωcm in an hour. Turning to the X-ray diffraction analysis, the crystal structure at 6.8 GPa after the temperature is decreased to r.t. is assigned to the same cubic structure ($Pm\bar{3}m$) with a = 5.373 Å. Moreover, the structure at r.t. after the release of pressure is also assigned to the cubic structure ($Pm\bar{3}m$) with a = 5.871 Å.

Considering the irreversibility of the phase transition and the discontinuous change of the unit cell volume, the tetragonal (II)-to-cubic phase transition is of first order.

Figure 8 shows the P−T phase diagram of $Cs_2Au_2I_6$, where three phases (i.e. phase I, tetragonal I; phase II: tetragonal II, phase III: cubic) exist. In connection with the P−T phase diagram, the following should be mentioned. In order to obtain the precise phase boundary, a sufficiently long interval time is necessary in the vicinity of the structural phase transition. However, because of the limited machine time, the mean measuring time per one point in the phase diagram and the interval time were about 15 and 20 min, respectively. The mixture of two or three phases in the vicinity of the phase boundary shown in Figure 8 is due to the nonequilibrium effect and the distribution of pressure and/or temperature in the sample. These are unavoidable problems under extreme conditions.

$Cs_2Au_2Br_6$. X-ray diffraction patterns of $Cs_2Au_2Br_6$ were measured in the region of a.p. to 11.2 GPa and r.t. to 215 °C.

Figure 9 shows the pressure dependence of the lattice constants, a and c, at r.t. With increasing pressure up to 8.2 GPa, the lattice constant, a, decreases monotonously showing a concave curvature. On the other hand, the lattice constant, c, decreases showing a concave curvature in the pressure region up to about 7 GPa and then decreases more rapidly showing a convex curvature with increasing pressure up to 8.2 GPa. As seen in Figure 9, a tetragonal-to-tetragonal phase transition takes place at about 9 GPa, where the c-axis contracts strikingly while

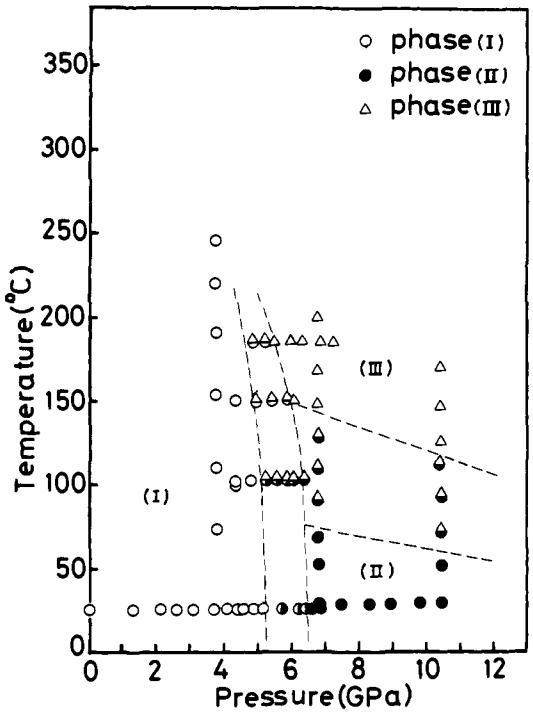

Figure 8. P−T phase diagram of $Cs_2Au_2I_6$: (I) tetragonal I phase; (II) tetragonal II phase; (III) cubic phase.

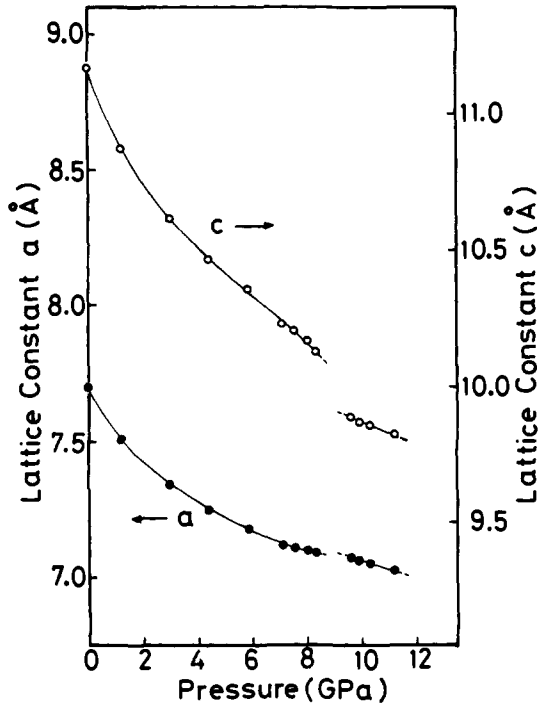

Figure 9. Pressure dependence of the lattice constants of $Cs_2Au_2Br_6$ at r.t.

the a-axis elongates slightly. Above the transition pressure, both the a- and c-axes contract monotonously with increasing pressure.

Figure 10 shows the pressure dependence of the relative volume with respect to the unit-cell volume at a.p. At the transition pressure, the normalized volume drops by 1%.

Figure 11 shows the pressure dependence of the axial ratio $2^{1/2}a/c$ of $Cs_2Au_2Br_6$ at r.t. With increasing pressure, $2^{1/2}a/c$ increases monotonously in the pressure region between a.p. and 7 GPa, and at about 7 GPa, where the activation energy for the electrical resistivity becomes zero,[12] the gradient of $2^{1/2}a/c$

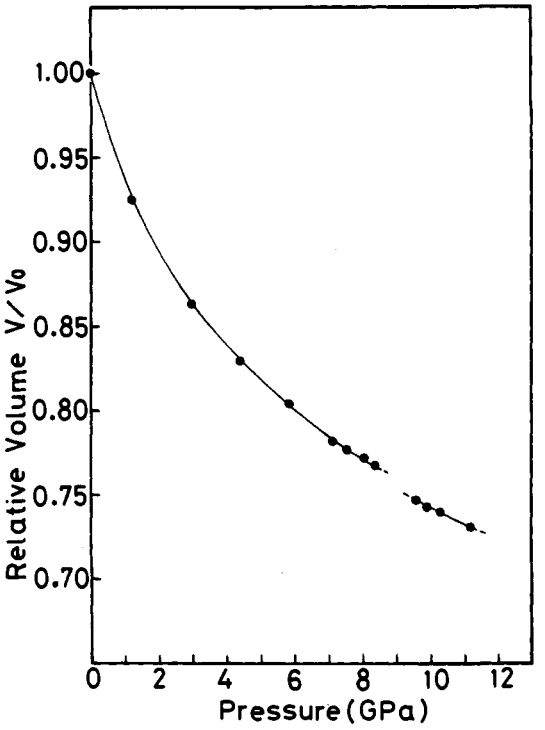

Figure 10. Pressure dependence of the volume of $Cs_2Au_2Br_6$ at r.t. The volume is normalized by that (V_0 = 662.70 Å^3) at a.p.

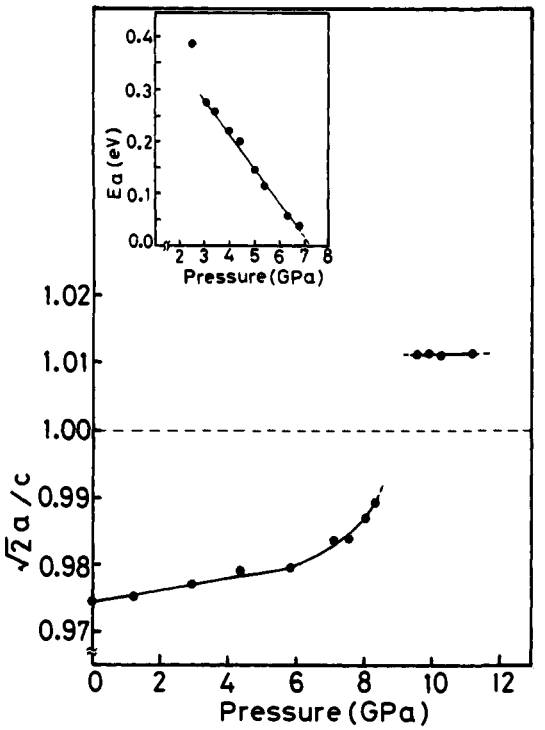

Figure 11. Pressure dependence of the axial ratio $2^{1/2}a/c$ of $Cs_2Au_2Br_6$ at r.t. The inset shows the activation energy of $Cs_2Au_2Br_6$ as a function of pressure (ref 11).

suddenly becomes steep. In the pressure region above 7.2 GPa, the HOMO of Au^I and the LUMO of Au^{III} overlap each other and the difference between the oxidation states of Au^I and Au^{III} would become small, which is presumably responsible for the remarkable increase in $2^{1/2}a/c$ above 7 GPa. At about 9 GPa, the axial ratio $2^{1/2}a/c$ jumps and passes over 1.00, and then it remains almost unchanged in the pressure region between 9.6 and 11.2 GPa. The pressure dependence of the axial ratio $2^{1/2}a/c$ in $Cs_2Au_2Br_6$ is quite different from that in $Cs_2Au_2I_6$.

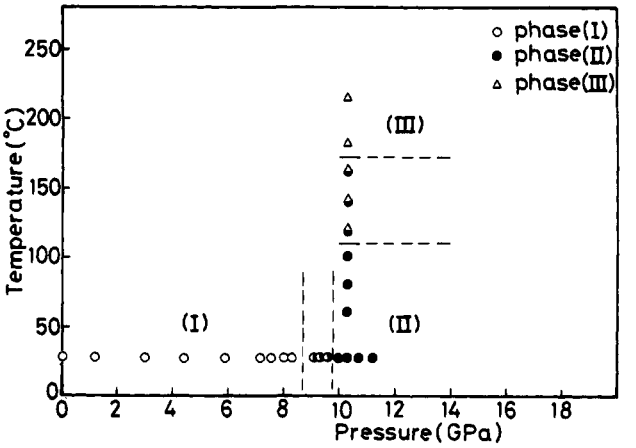

Figure 12. P–T phase diagram of $Cs_2Au_2Br_6$: (I) tetragonal I phase; (II) tetragonal II phase; (III) cubic phase.

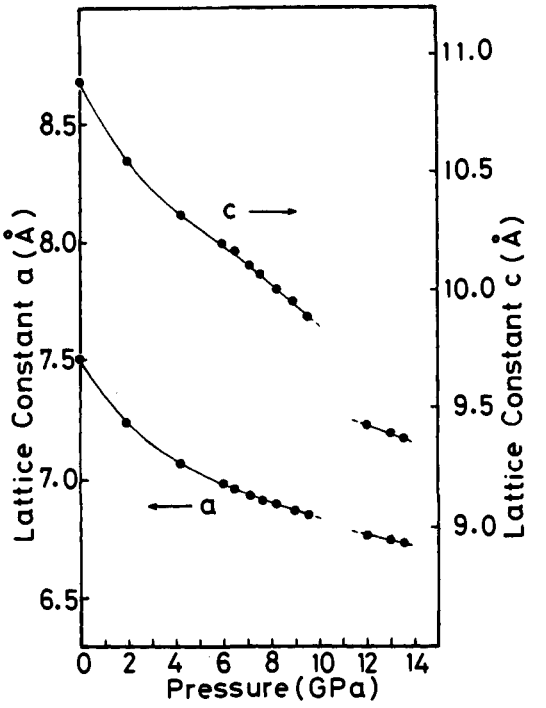

Figure 13. Pressure dependence of the lattice constants of $Cs_2Au_2Cl_6$ at r.t.

The P–T phase diagram of $Cs_2Au_2Br_6$ is shown in Figure 12. The cubic phase could be obtained as a metastable state even at r.t. and a.p. in a manner similar to that in $Cs_2Au_2I_6$.

$Cs_2Au_2Cl_6$. X-ray diffraction patterns of $Cs_2Au_2Cl_6$ were measured in the region of a.p. to 13.5 GPa and r.t. to 316 °C.

Figure 13 shows the pressure dependence of the lattice constants, *a* and *c*, at r.t. With increasing pressure up to 7 GPa, the lattice constant, *c*, first decreases showing a concave curvature and then decreases more rapidly showing a convex curvature between 7 and 9.5 GPa. On the other hand, the lattice constant, *a*, decreases monotonously showing a concave curvature in the pressure region up to 9.5 GPa. As seen in Figure 13, a tetragonal-to-tetragonal phase transition occurs at about 11 GPa, where the *a*- and *c*-axes contract discontinuously. Above the transition pressure, both the *a*- and *c*-axes contract monotonously with increasing pressure.

Figure 14 shows the pressure dependence of the relative volume with respect to the unit-cell volume at a.p. At the transition pressure, the normalized volume drops by about 3%. Above 11 GPa, the gradient of the volume contraction becomes small.

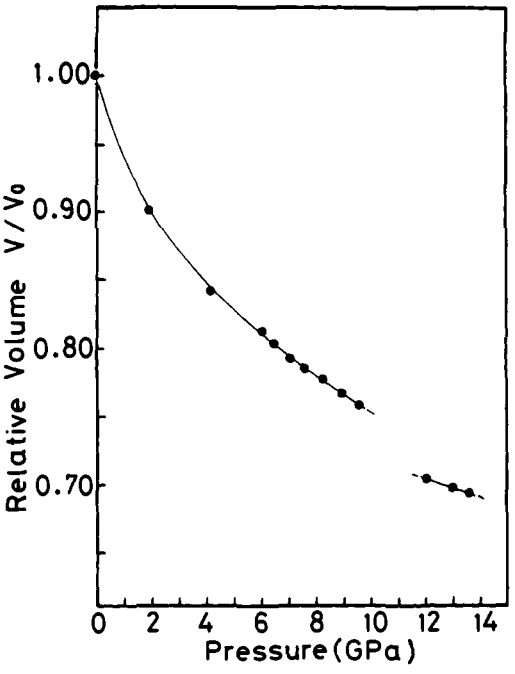

Figure 14. Pressure dependence of the volume of $Cs_2Au_2Cl_6$ at r.t. The volume is normalized by that (612.56 Å^3) at a.p.

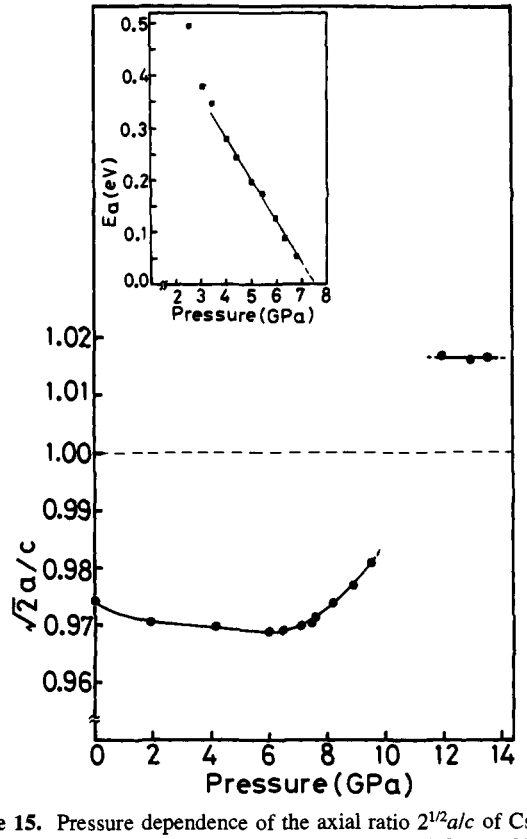

Figure 15. Pressure dependence of the axial ratio $2^{1/2}a/c$ of $Cs_2Au_2Cl_6$ at r.t. The inset shows the activation energy of $Cs_2Au_2Cl_6$ as a function of pressure (ref 11).

Figure 15 shows the pressure dependence of the axial ratio $2^{1/2}a/c$ of $Cs_2Au_2Cl_6$ at r.t. For the case of $Cs_2Au_2Cl_6$, which is different from $Cs_2Au_2Br_6$ and $Cs_2Au_2I_6$. $2^{1/2}a/c$ slightly decreases with increasing pressure up to about 7 GPa. Above 7.5 GPa, the axial ratio remarkably increases with pressure. As seen in the inset of Figure 15, the abrupt increase in $2^{1/2}a/c$ above 7.5 GPa is due to the overlapping of the HOMO of Au^I and the LUMO of Au^{III}, as described for the case of $Cs_2Au_2Br_6$. At about 11 GPa, the axial ratio $2^{1/2}a/c$ jumps and passes

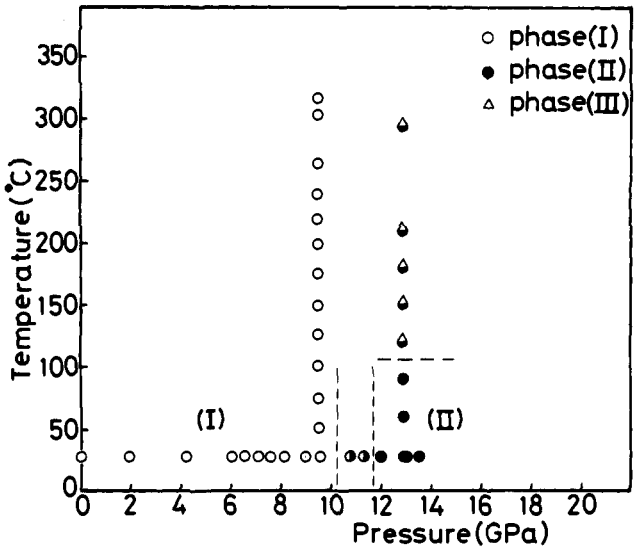

Figure 16. P−T phase diagram of $Cs_2Au_2Cl_6$: (I) tetragonal I phase; (II) tetragonal II phase; (III) cubic phase.

over 1.00, and then it remains almost unchanged up to 13.5 GPa. On the whole, the pressure dependence of the axial ratio $2^{1/2}a/c$ in $Cs_2Au_2Cl_6$ resembles that in $Cs_2Au_2Br_6$.

When the temperature is increased at 12.9 GPa, the (002) and (004) reflections begin to diminish above 120 °C without a change in their energy positions. This behavior of the (002) and (004) reflections of $Cs_2Au_2Cl_6$ is similar to that of the (002) and (004) reflections of $Cs_2Au_2I_6$ in the process of the tetragonal II-to-cubic phase transition. From the analogy to the tetragonal II-to-cubic phase transition in $Cs_2Au_2I_6$, it is considered that $Cs_2Au_2Cl_6$ begins to undergo the tetragonal II-to-cubic phase transition at 12.9 GPa and 120 °C.

The P−T phase diagram of $Cs_2Au_2Cl_6$ is shown in Figure 16.

Discussion

As mentioned above, we have obtained the P−T phase diagram for $Cs_2Au_2X_6$ (X = Cl, Br, and I), where two kinds of tetragonal phases and a cubic phase exist. Both the pressure-induced tetragonal I-to-tetragonal II transition and the temperature-induced tetragonal II-to-cubic transition are of first order. The cubic phase appearing at high pressures and high temperatures can be obtained as a metastable state even at r.t. and a.p.

Tetragonal-to-Tetragonal Transition. At r.t., $Cs_2Au_2Cl_6$, $Cs_2Au_2Br_6$, and $Cs_2Au_2I_6$ undergo a tetragonal-to-tetragonal phase transition at 11, 9, and 5.5 GPa, respectively, whose values are beyond the pressure where the semiconductor-to-metal transition takes place. The pressures where the activation energies become zero are 7.5, 7.2, and 4.5 GPa for $Cs_2Au_2Cl_6$, $Cs_2Au_2Br_6$, and $Cs_2Au_2I_6$, respectively.[12] Above the pressure where the activation energy becomes zero, the valence states of Au^I and Au^{III} closely approach the Au^{II} state, which is proven by the fact that the (211) and (103) reflections, caused by the distortion of the bridging halogens from the midpoint between the Au^I and Au^{III} ions, are hardly detected in this pressure region. If the valence states of Au^I and Au^{III} finally become $Au^{II}(5d^9)$, the lowering in symmetry of AuX_6 octahedra should be caused by the Jahn−Teller effect.

Therefore, the tetragonal-to-tetragonal phase transition in $Cs_2Au_2X_6$ is regarded as a cooperative Jahn−Teller transition driven by the $Au^{I,III} \rightarrow Au^{II}$ transition. In connection with this, very recently, we have proven by means of ^{197}Au Mössbauer

spectroscopy under high pressure[23] that the Au valence state of the second tetragonal phase in $Cs_2Au_2I_6$ is Au^{II}.

Second Tetragonal Phase. In the second tetragonal phase, the reflections caused by the distortion of the halogens from the midpoint of the Au ions practically disappear. Therefore, the space group of the second tetragonal phase is regarded as *P4/mmm*, where all the bridging halogens are located at the midpoint of the Au ions and the Au valence state is $Au^{II}(5d^9)$.

Above the transition pressure, $2^{1/2}a/c$ of $Cs_2Au_2I_6$ is smaller than 1.00 and its decreases with pressure. On the other hand, $2^{1/2}a/c$ of $Cs_2Au_2X_6$ (X = Cl and Br) is larger than 1.00 and it remains almost unchanged. Therefore, in the second tetragonal phase, the AuI_6 octahedra in $Cs_2Au_2I_6$ are "elongated", while the AuX_6 octahedra in $Cs_2Au_2X_6$ (X = Cl and Br) are "compressed".

Considering the distortion pattern of the AuX_6 octahedra, the HOMO in the second tetragonal phase is the half-filled $5d_{z2}$ band and the half-filled $5d_{x2-y2}$ band for $Cs_2Au_2X_6$ (X = Cl and Br) and $Cs_2Au_2I_6$, respectively. Therefore, it is considered that the second tetragonal phase in $Cs_2Au_2X_6$ (X = Cl and Br) behaves as a one-dimensional conductor, while that in $Cs_2Au_2I_6$ behaves as a two-dimensional conductor. In fact, we have confirmed that the second tetragonal phase in $Cs_2Au_2I_6$ behaves as a two-dimensional conductor.[18]

Strictly speaking, the single-crystal X-ray analysis under high pressure is necessary to elucidate the detailed crystal structure of the second tetragonal phase, and this study is in progress.

Cubic Phase. The space group of the cubic phase is regarded as $Pm\bar{3}m$, where the Au valence state is $Au^{II}(5d^9)$ and HOMO is the degenerate $5d_{x2-y2}$ and $5d_{z2}$ bands with three-quarters filling.

(23) Hafner, S. S.; Kojima, N.; Stanek, J.; Zhang, Li *Phys. Lett. A* **1994**, *192*, 385–388.

The tetragonal II-to-cubic phase transition can be interpreted as follows. Under high temperatures, due to the entropy term, the free energy of the cubic phase is lower than that of the distorted one. Therefore, as the temperature is raised, the Jahn–Teller distorted structure undergoes a transformation of crystal lattice into the cubic structure.

Au Valence State and Transport Phenomena. In the relationship between the Au valence state and the transport phenomena of $Cs_2Au_2X_6$, the following should be mentioned.

Recently, we have investigated the single-crystal resistivity of $Cs_2Au_2I_6$ as a function of temperature at various pressures up to 8 GPa.[17]

In the pressure region between 3 and 5 GPa, where the Au valence state is vigorously fluctuating between Au^{I} and Au^{III}, several anomalous peaks and shoulders appear in the resistivity around 200 and 100 K. Especially, the resistivity peak at about 100 K appears above 4.5 GPa, and it is strikingly enhanced as the pressure approaches the tetragonal-to-tetragonal transition point. However, in the second tetragonal phase, these anomalous resistivity peaks completely disappear.

These phenomena strongly support the theory that the valence state of Au changes at the tetragonal-to-tetragonal transition and this structural transition is driven by the $Au^{I,III} \rightarrow Au^{II}$ transition. The Au valence fluctuation is presumably responsible for the anomalous resistivity peaks in $Cs_2Au_2I_6$ under low temperatures in the pressure region between 3 and 5 GPa.

Acknowledgment. The authors thank Dr. W. Utsumi for his help with the high pressure apparatus. We are also indebted to Dr. H. Sato and Mr. A. Tanaka for their help with the X-ray diffraction measurement under high pressures. This study was partly supported by the Grant-in-Aid for Scientific Research from the Ministry of Education, Science and Culture, Japan, and the Iwatani Naoji foundation.